Astronomy
& Astrophysics

Spectral fits to the 1999 Aql X-1 outburst data

T. J. Maccarone[1] and P. S. Coppi[2]

[1] Astrophysics Sector, SISSA/ISAS, via Beirut No. 2–4, 34014, Trieste, Italy
[2] Department of Astronomy, Yale University, PO Box 208101, New Haven CT 06520-8101, USA
   e-mail: coppi@astro.yale.edu

Abstract. We present analysis and spectral fits of the RXTE data from the May/June 1999 outburst of Aql X-1. These data include observations in the rising portion of the hard state, in the soft state, and in the falling portion of the hard state. We show that the data can be fit by a purely thermal Comptonization model for all the observations, but that more complicated models cannot be ruled out. Up to 60% of the corona's power in the soft state may be injected into non-thermal electrons. The soft state data show approximately constant optical depth and coronal temperatures over a range of ~10 in luminosity, while they show evidence for a reduction of seed photon temperature with reduced luminosity and indicate that the characteristic size of the seed photon emitting region is roughly constant throughout the soft state. The hard state before the soft state shows a higher luminosity, higher optical depth, and lower electron temperature than the hard state after the soft state. We find a reduction of the hard (30–60 keV) X-ray flux during a type I burst and show that it requires a total corona energy reservoir of less than ~10^{38} ergs.

Key words. accretion, accretion disks – radiation mechanisms: non-thermal – X-rays: individual: Aql X-1 – X-rays: bursts

1. Introduction

The lightcurves of X-ray transients have revealed an outburst cycle consisting of several spectral states – an off/quiescent state where the luminosity is low and the spectrum is difficult to measure, a low/hard state, characterized by a power law with photon index $\Gamma < 2$, presumably coming from Comptonization of photons in a hot, optically thin medium, a high/soft state, characterized by a quasi-thermal spectrum, consistent with the emission from an accretion disk with a peak temperature of ~10^7 K, often accompanied by a weak power law tail, and a very high state, consisting of a strong thermal accretion disk component plus a power law tail of comparable or greater luminosity (see Nowak 1995 for a review of the characteristics of the spectral states). Additionally, the transition between the hard and soft states is sometimes classified as a separate "transition state".

Two broad classes of mechanisms have been invoked to explain the transitions between spectral states in black hole transients. In one mechanism, a two temperature accretion flow is proposed to explain the hard state. A transition radius between the cool, geometrically thin, optically thick outer disk and the hot, optically thin, geometrically thick inner corona changes with accretion rate, yielding a pure disk spectrum at high luminosity and a Comptonized spectrum at lower luminosity (see e.g. Narayan & Yi 1995; Meyer et al. 2000).

Alternatively, the differences between the spectral states may be explained in terms of differing scale heights above the disk for magnetically active hot regions in the hard state and the soft state (see e.g. di Matteo et al. 1999; Nayakshin & Svensson 2001). The fraction of the luminosity supplied to the corona must also change during the state transitions. Relatively little work has been done to explain why this should occur at different luminosities.

In neutron star systems, a propeller mechanism has sometimes been invoked to explain state transitions (see e.g. Lamb et al. 1973; Zhang et al. 1998). In this model, when the magnetospheric radius of the neutron star (i.e. the radius where the ram pressure of the accreting gas matches the magnetic pressure of the accreting star) is outside the corotation radius of the neutron star, then accreting matter is driven away from the neutron star by the magnetic pressure and a hard state sets in. The low luminosities (~10^{33} ergs/s) seen in quiescence in Aql X-1 suggest that some kind of outflow must be present in that state and that the propeller is a likely mechanism (Campana et al. 1998). What is not certain is whether the magnetic field is large enough to cause the onset of the propeller effect at the luminosities of the state transitions.

Past studies of X-ray transients have focused on the broadband spectra in quiescence (Yi et al. 1996), X-ray luminosities in quiescence (see e.g. Garcia et al. 2001), and time delays between optical and X-ray rises in outburst (see e.g. Jain et al. 2001). Aql X-1 has been a well studied source because it shows a fairly regular outburst cycle with a periodicity of

Table 1. The RXTE observations analyzed for this work. Dates are presented in DD/MM/YY format.

Obs Id	Start Date	Start Time	Stop Date	Stop Time	JD-2 451 300
40049-01-02-00	15/05/99	17:23:04	15/05/99	18:37:15	13
40049-01-02-01	16/05/99	20:50:20	16/05/99	21:32:15	14
40049-01-02-02	17/05/99	22:29:22	17/05/99	23:06:15	15
40047-01-01-00	18/05/99	20:41:23	18/05/99	21:20:15	16
40047-01-01-01	19/05/99	22:24:23	19/05/99	23:04:15	17
40047-02-01-00	22/05/99	15:39:59	22/05/99	19:33:15	20
40047-02-02-00	23/05/99	18:59:08	23/05/99	22:59:15	21
40047-02-03-00	24/05/99	17:10:15	24/05/99	21:22:15	22
40047-02-03-01	26/05/99	17:11:36	26/05/99	17:34:47	24
40047-02-04-00	29/05/99	15:30:06	29/05/99	19:40:15	27
40047-02-05-00	31/05/99	15:29:23	31/05/99	19:58:15	29
40047-03-01-00	02/06/99	13:46:15	02/06/99	18:41:15	31
40047-03-02-00	03/06/99	15:25:26	03/06/99	20:49:15	32
40047-03-03-00	04/06/99	13:47:17	04/06/99	18:36:15	33
40047-03-04-00	05/06/99	07:21:37	05/06/99	09:57:15	34
40047-03-06-00	07/06/99	12:07:50	07/06/99	16:54:15	36
40047-03-07-00	08/06/99	12:06:42	08/06/99	13:51:05	37
40047-03-08-00	09/06/99	15:17:18	09/06/99	18:26:15	38
40047-03-09-00	11/06/99	15:15:53	11/06/99	16:32:15	40

about 300 days. It has been shown to be an atoll source (Cui et al. 1998; Reig et al. 2000). It has been the subject of optical monitoring in quiescence (Jain 2001), and the optical rise was used to trigger the pointed X-ray observations at a lower flux than the sensitivity of the All Sky Monitor on the Rossi X-ray Timing Explorer allows (Bradt et al. 1993). The X-ray data triggered by the optical flare have allowed the analysis of an X-ray lightcurve from a single outburst starting in the low/hard state, entering the high/soft state, and returning to the low/hard state; similar work to ours has been done recently for 4U 1704-44 without optical triggering (Barret & Olive 2002).

2. Observations

Aql X-1 was monitored by the RXTE pointed instruments during May and June of 1999, caught early in the rising phase of its outburst due to optical monitoring used to trigger the pointed observations (Jain 2001). The observation times analyzed in this paper are listed in Table 1. A few additional observations have been omitted because there were problems with the HEXTE background subtraction or because the flux levels were too low for accurate spectral fits. For each observation, the data were extracted using the standard RXTE screening criteria for earth elevation and time since the last South Atlantic Anomaly passage. The number of Proportional Counter Units turned on varied, so the time interval used was chosen to maximize the total integrated effective area times exposure time while still allowing for a single set of PCUs to be used. The HEXTE data are also extracted according to the standard RXTE screening procedures. For the observations where Type I X-ray bursts are seen, the bursts are excluded from the integration so as not to contaminate the spectrum. The HEXTE data are rebinned to have three bins per channel from channel 16 to channel 21, 5 bins per channel from channel 22 to 51, 15 bins per channel

from channel 52 to 126, and 24 bins per channel from channel 127 to 198. The fits include PCA data from 3.0 to 20.0 keV and HEXTE data from 17.0 to 190.0 keV, corresponding to the energy ranges where the two instruments are generally considered reliable.

3. Analysis

3.1. Data reduction

The data are then fit with a thermal Comptonization model within XSPEC 10.0 (the eqpair model, with the electrons required to be put purely into the thermal component – see Sect. 3.2 below for a description of the model), plus a Gaussian component to represent the contributions of an iron line, multiplied by a photoelectric absorption component (wabs). The purely thermal version of this model is chosen as the simplest one that fits the data well and gives some insight about which physical parameters are varying. A hybrid thermal/non-thermal version of the model is also fit to the data later on. The neutral hydrogen column density is frozen to 3.4×10^{21} cm^{-2}, the Galactic value along the line of sight to Aql X-1. A 1% systematic error is added to all channels from both the PCA and the HEXTE. The overall normalization of the HEXTE data is allowed to float and varies by about 30%. The Gaussian component is required to have an energy between 6.2 and 7.0 keV and a physical width of less than 1.2 keV. For most of the observations, the presence of the line is only marginally statistically significant. Given the slightly larger systematic errors near the iron line than in the rest of the RXTE spectrum and that these errors tend to make the measured flux in this region larger than that measured with other instruments, we view the measurements of the line with skepticism, omit the parameters of the line measurements from the tables and refrain from discussing any implications they might have; while the formal statistical

significance of the line is high, it is possible that the fits are responding to errors in the response matrix.

3.2. The Comptonization model

The EQPAIR model calculates a self-consistent temperature and pair optical depth for the hot electron corona. It allows for injection of energy into the coronal electrons in both a Maxwellian distribution ("thermal Comptonization") and a power law distribution ("non-thermal Comptonization"). It then solves for a final electron distribution based on the relative heating and cooling rates of the electrons due to radiative processes and Coulomb interactions, so the electron temperature is not an explicit parameter, but is instead computed self-consistently. It allows for Compton reflection, but does not self-consistently compute the line emission from reflection. It assumes a spherical geometry with the seed photons initially distributed uniformly. We choose this model because it is versatile (allowing for both thermal and non-thermal injection and allowing for Compton reflection) and runs relatively quickly given its complexity.

The basic parameters of the thermal Comptonization component of the model are a thermal electron compactness (equal to the luminosity injected into the Maxwellian component of the hot electron distribution times the Thomson cross-section and divided by the product of the electron rest energy, the speed of light and the radius of the corona), and optical depth, and a seed photon temperature. The temperature of the corona is an implicit one determined by the energy balance between the heating rate and cooling rate of the corona. The compactness of the seed photon distribution is frozen to unity, so the thermal electron compactness, ℓ_{th} is really the ratio of the coronal luminosity to the seed photon luminosity. Barring an independent estimate of the corona's size, the strongest constraints on the total compactness will come from annihilation line measurements, which are not possible given that our observations extend only to 190 keV. For a more detailed description of the model, we refer the reader to Coppi (1999).

3.3. Brief overview of results

The results of the spectral fitting are presented in Table 2 and plotted in Fig. 1. The important implicit parameters – the luminosity in the soft component, the luminosity in the corona, and the temperature of the corona – are plotted in Fig. 2. The fluxes are converted to luminosities assuming a distance to Aql X-1 of 2.5 kpc (Chevalier et al. 1999), although we note that this distance measurement has been disputed by Rutledge et al. (2001), who claim a minimum distance of 4 kpc and a most likely distance of 4.7 kpc. The relative luminosities of the soft component and coronal component are computed by multiplying the total luminosity by the fraction of the total compactness in each component. From inspection of Table 2, it seems that the source entered the soft state on May 22 and remained there through June 7 (JD 2 451 320 through 2 451 338). These dates could be in error by a few days due to data gaps. In the hard state, the optical depths range from ~1–4 and the coronal
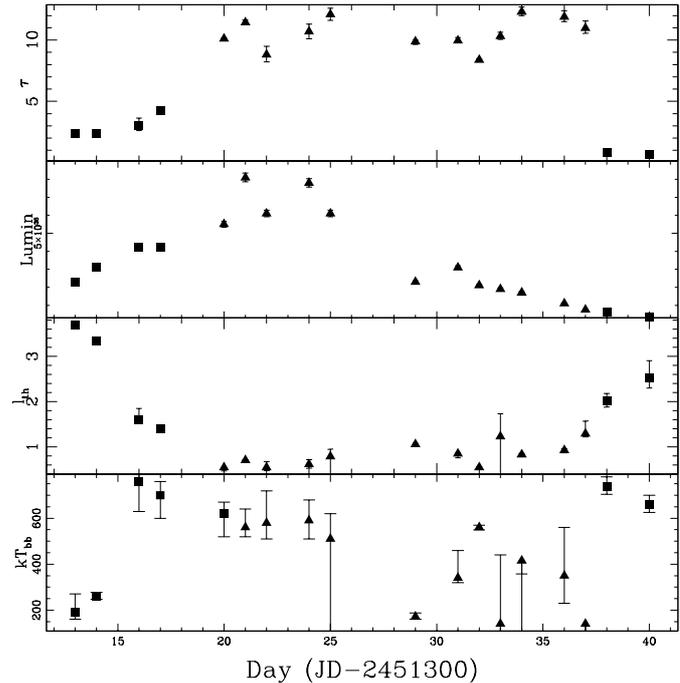

Fig. 1. The spectral fit parameters plotted versus the observation date. From top to bottom: the optical depth, the luminosity in ergs/s/cm², the thermal compactness, and the blackbody temperature in eV. In all panels, the filled squares show the observations we have defined to the hard state and the filled triangles show the observations we have defined to be the soft state.

temperatures range from ~10–200 keV (a typical hard state spectrum is plotted in Fig. 2). In the soft state, the coronal optical depths are ~10 and the temperatures are ~2.5 keV. Two different model fits to a typical soft state spectrum are presented in Fig. 3, while a typical hard state spectrum is plotted in Fig. 4.

4. Discussion

4.1. Robustness of fits and alternative models

Previous work has attempted to fit the data as coming from a disk blackbody model plus a Comptonized blackbody (Mitsuda et al. 1984; Barret et al. 2002). We find that for some hard state observations, the addition of a second blackbody component can give a slight improvement to the goodness of fit, and results in a slightly higher coronal temperature and lower optical depth, as well as significant changes in the iron line flux. However, since the fits are satisfactory with a single Comptonized blackbody, and the additional blackbody generally represents less than ~20% of the 2–200 keV flux, we use the simpler single Comptonized blackbody model. In general, RXTE is not capable of distinguishing between the different models for the soft flux or between the disk and boundary layer components because it has relatively poor spectral resolution at energies below 5 keV and has no coverage below 2 keV. Observations from instruments such as BeppoSax or XMM-Newton are more useful for making such measurements. Furthermore, we note that the soft photon temperatures derived with RXTE may be subject to significant systematic errors
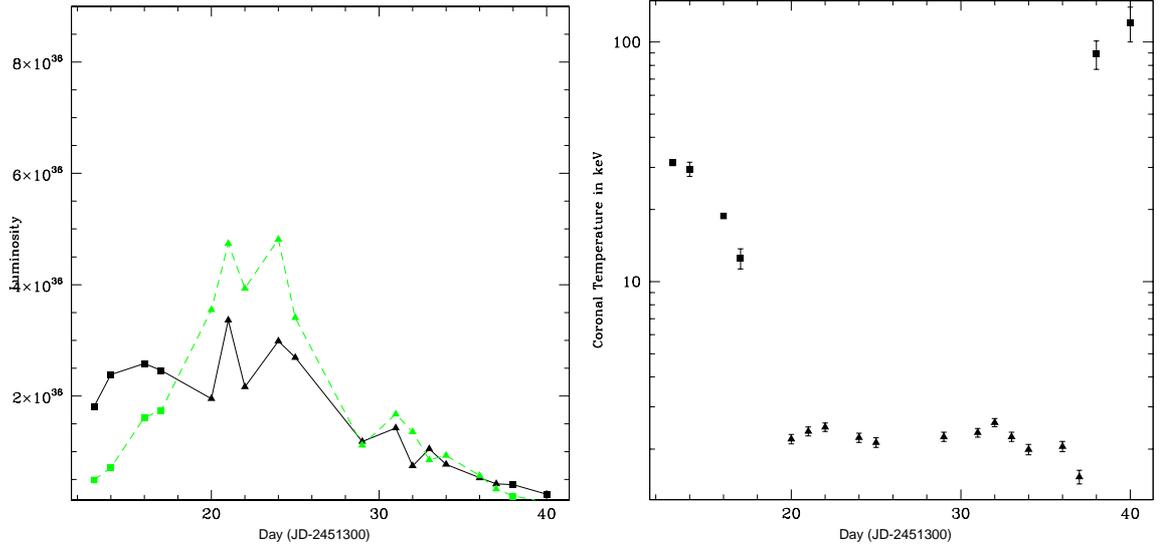
Fig. 2. a) The upscattered luminosity (solid line) and the seed photon luminosity (dashed line) plotted versus day. **b)** The coronal temperature plotted versus day. In both plots, the filled squares show the observations we have defined to the hard state and the filled triangles show the observations we have defined to be the soft state.

Table 2. The best fit parameter values for the thermal Comptonization fits to the Aql X-1 outburst data. Double asterisks represent parameters whose error bars were either too large to be fit (a factor of three or more from the best fit value), or were large enough to exceed the hard bounds placed on the parameters. There are 59 degrees of freedom for each observation. The columns are: Obs ID – the RXTE observation ID number, kT_{bb} – the seed photon temperature in eV, ℓ_{th} – the thermal compactness of the corona, τ – the optical depth of the corona, L – the total luminosity of the source, assuming a 2.5 kpc distance, and χ^2/ν, the reduced χ^2 from the spectral fits.

Obs ID	kT_{bb}	ℓ_{th}	τ	L	χ^2/ν
40049-01-02-00	$190\pm^{80}_{30}$	$3.69\pm^{.08}_{.06}$	$2.40\pm^{.07}_{.05}$	2.3×10^{36}	1.73
40049-01-02-01	$260\pm^{18}_{12}$	$3.34\pm^{.07}_{.06}$	$2.39\pm^{.13}_{.06}$	3.1×10^{36}	1.75
40049-01-02-02	$260\pm^{18}_{12}$	$3.34\pm^{.07}_{.06}$	$2.39\pm^{.13}_{.06}$	3.9×10^{36}	1.36
40047-01-01-00	$760\pm^{70}_{130}$	$1.60\pm^{.25}_{.07}$	$3.02\pm^{.62}_{.40}$	4.2×10^{36}	0.72
40047-01-01-01	$700\pm^{60}_{100}$	$1.41\pm^{.06}_{.08}$	$4.23\pm^{.23}_{.18}$	4.2×10^{36}	0.84
40047-02-01-00	$620\pm^{50}_{100}$	$0.55\pm^{.08}_{.08}$	$10.12\pm^{.06}_{.08}$	5.5×10^{36}	1.00
40047-02-02-00	$560\pm^{80}_{40}$	$0.71\pm^{.01}_{.01}$	$11.45\pm^{.19}_{.20}$	8.1×10^{36}	0.63
40047-02-03-00	$580\pm^{140}_{70}$	$0.55\pm^{.13}_{.07}$	$8.82\pm^{.68}_{.60}$	6.1×10^{36}	0.84
40047-02-03-01	$590\pm^{90}_{80}$	$0.62\pm^{.10}_{.09}$	$10.70\pm^{.6}_{.6}$	7.8×10^{36}	0.55
40047-02-04-00	$510\pm^{110}_{**}$	$0.79\pm^{.16}_{**}$	$12.10\pm^{0.5}_{0.5}$	6.1×10^{36}	0.61
40047-02-05-00	$172\pm^{15}_{12}$	$1.06\pm^{.02}_{.02}$	$9.88\pm^{.12}_{.24}$	2.3×10^{36}	0.99
40047-03-01-00	$340\pm^{120}_{20}$	$0.85\pm^{.02}_{.09}$	$9.95\pm^{.25}_{.15}$	3.1×10^{36}	0.84
40047-03-02-00	$560\pm^{10}_{10}$	$0.55\pm^{.01}_{.01}$	$8.38\pm^{.10}_{.12}$	2.1×10^{36}	1.68
40047-03-03-00	$140\pm^{300}_{**}$	$1.23\pm^{.5}_{**}$	$10.31\pm^{.34}_{.26}$	1.9×10^{36}	1.10
40047-03-04-00	$420\pm^{**}_{60}$	$0.83\pm^{.03}_{.03}$	$12.29\pm^{.40}_{.26}$	1.7×10^{36}	0.80
40047-03-06-00	$350\pm^{210}_{120}$	$0.93\pm^{.03}_{.06}$	$11.86\pm^{.50}_{.43}$	1.1×10^{36}	1.06
40047-03-07-00	$140\pm^{**}_{**}$	$1.29\pm^{.28}_{.07}$	$10.99\pm^{.57}_{.44}$	7.5×10^{35}	0.67
40047-03-08-00	$740\pm^{40}_{35}$	$2.02\pm^{.16}_{.14}$	$0.84\pm^{.10}_{.07}$	6.1×10^{35}	0.58
40047-03-09-00	$660\pm^{40}_{35}$	$2.52\pm^{.38}_{.22}$	$0.69\pm^{.14}_{.11}$	3.3×10^{35}	0.80

because they are determined predominantly by the lowest energy channels which have relatively high systematic errors.

Under the assumption that the EQPAIR model is a correct description of the data, it is potentially sensitive to changes in the seed photon temperature even when the seed photon distribution has dropped off significantly by the lower bound of the observed energy range. The reason is that the broad bump of the seed photons must join smoothly to the "power law" that comes out of analytic calculations assuming a delta function seed photon distribution. Thus there is some curvature at low energies which deviates from the idealized power law description, and this curvature constrains the seed photon temperature. In fact, this is a generic property of numerically computed Comptonization models. Similar results have been found by Nowak et al. (2002) for GX 339-4 fits. We caution that systematic errors in the RXTE response matrix and in the neutral hydrogen column are likely to cause systematic errors in the temperature measurements for all sources. For neutron
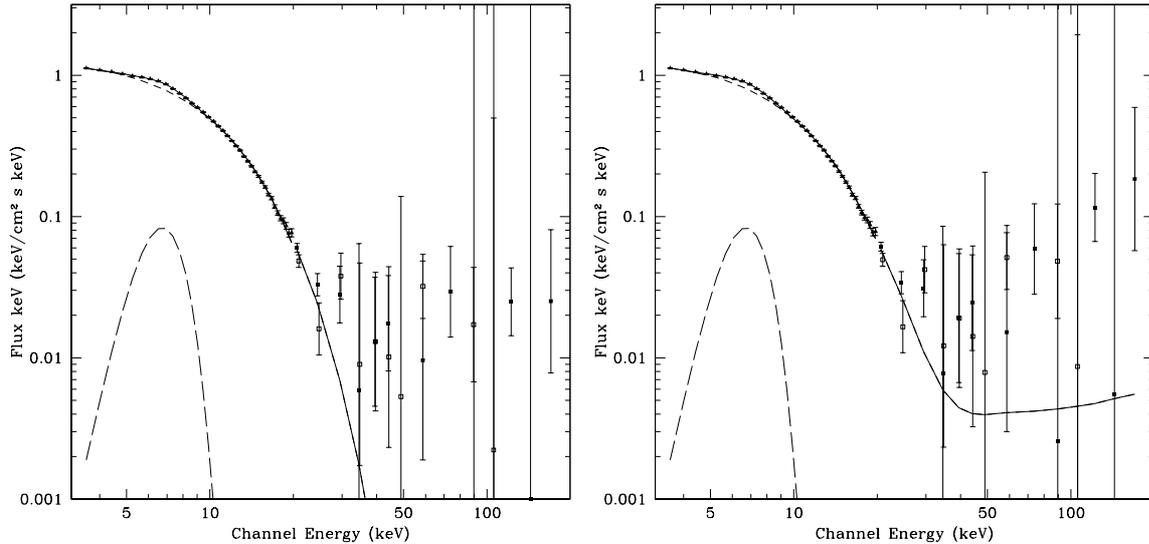
Fig. 3. The fits to soft state data (ObsID 40047-03-01-00) for Aql X-1. The figure to the left is that for the thermal model and to the right is for the hybrid model. The triangles are the PCA data, multiplied by 0.7 to match with the HEXTE data. The filled squares are HEXTE cluster 0 and the open squares are HEXTE cluster 1. The solid line represents the sum of the model components, the short-dashed line represents the EQPAIR contribution and the long-dashed line represents the Gaussian "iron line." Where no error bars are visible, the errors are smaller than the size of the data point.

star sources, the possible existence of two seed photon components (one from the star's surface and one from the disk) complicates matters further. We do believe that systematic trends in the seed temperatures are meaningful (i.e. where there is statistically significant evidence that the temperature in observation A is higher than that in observation B, we do believe that it is, in fact, higher), but we do not believe that RXTE is the best mission for making actual measurements of the temperature.

We also attempt to fit the data with thermal Comptonization plus Compton reflection. We find that the fits are unconstrained when the channels between 6 and 10 keV are ignored, implying that the fit is sensitive only to the edges and not to the curvature of the continuum. Since the edges depend sensitively on the RXTE response matrix and on whether one or two seed blackbody photon distributions are included, we believe little can be said about whether Compton reflection is important in these data.

The spectra in the soft state fit the canonical high optical depth, low temperature corona for a Comptonized blackbody that has been seen in other neutron star sources (e.g. di Salvo et al. 2001). It is of some interest to note that this spectral form matches both the Z source GX 349+2 and the atoll source Aql X-1 in its soft state, providing further evidence that the atoll/Z-source designation is somewhat arbitrary (see Muno et al. 2002). Within the soft state, the optical depth, coronal temperature, and seed photon temperature do not to show any trends, except that the lowest seed photon temperatures seem to be found after the large luminosity drop on JD 2 451 329. The best fitting disk temperature seems to drop by a factor of about 2 as the source drops in luminosity by a factor of about 10. Specifically, the first five observations in the soft state have disk temperatures of about 550 eV and luminosities in the range of 6–8×10^{36} ergs/s, while the later observations in the soft state generally have temperatures around 300 eV, with

luminosities in the range 1–3×10^{36} ergs/s. This presents evidence that the size of the region from which the seed photons come does not vary by more than a factor of about 2 in the soft state, as for a constant sized emission region, $T_{bb} \propto L^{1/4}$. Previous work on the black hole systems GRO J 1655-40 (Sobczak et al. 1999) and XTE J 1550-564 (Sobczak et al. 2000) has shown that their inner disk radii are likely to remain constant through the high/soft state as well. We stress that while the actual temperatures (and hence the actual size of the emission region) are susceptible to rather large systematic errors, the trends in the temperature should be much more reliable.

We also fit the soft state data with a hybrid thermal/non-thermal Comptonization model to determine whether there might be a power law tail to the electron energy injection function. We find that the data for a typical soft state observation (observation 40047-03-01-00) are consistent with up to 60% of the coronal luminosity injected into non-thermal electrons (i.e. electrons with a power law distribution), but the data are not good enough to distinguish between the models. The plots of the pure thermal electron distribution fit and the hybrid distribution fit are shown in Fig. 3, which shows weak evidence for an extended tail above 20 keV. We note that it does not appear that either model fits the HEXTE data well, but that the errors on the HEXTE data are quite large and that given the location of Aql X-1 in the disk of the Galaxy, activity of a foreground/background source cannot be ruled out as a possible cause for this extra hard X-ray emission. To date, such extended power law tails have been seen in black hole sources (see e.g. Gierlinski et al. 1999) and in Z source neutron stars (D'Amico et al. 2001; di Salvo et al. 2001), but not in atoll sources. These tails have been proposed as coming from non-thermal electron distributions (see e.g. Coppi 1999) or bulk motion Comptonization from the inner accretion flow (see e.g. Papathanassiou & Psaltis 2001). It has been argued that the
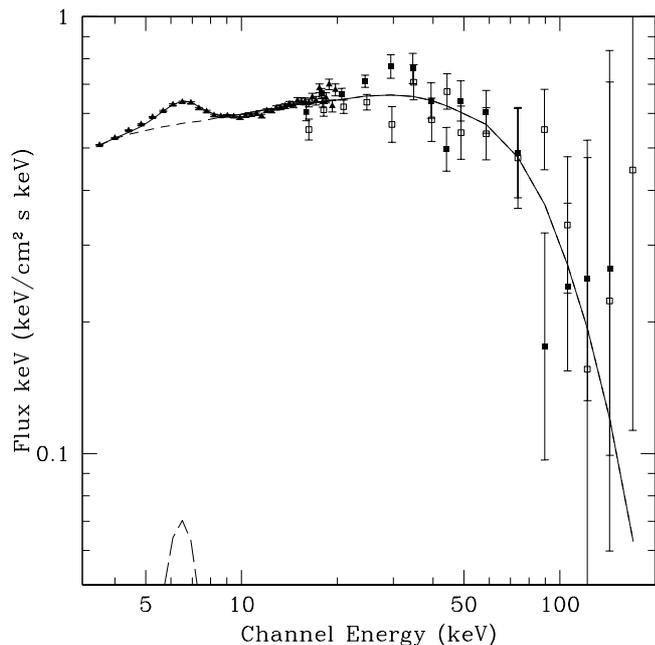
Fig. 4. The fit to the hard state data for Aql X-1. The observation chosen is 40049-01-02-02, shortly before the transition to the soft state. The triangles are the PCA data, multiplied by 0.7 to match with the HEXTE data. The filled squares are HEXTE cluster 0 and the open squares are HEXTE cluster 1. The solid line represents the sum of the model components, the short-dashed line represents the EQPAIR contribution and the long-dashed line represents the Gaussian "iron line." Where no error bars are visible, the errors are smaller than the size of the data point.

presence of an extended tail is a definitive signature of strong gravity and hence of the presence of a black hole (Titarchuk & Zannias 1998). Since it could be argued that the non-thermal tails seen in Z sources are related to the stars' relatively strong magnetic fields (see e.g. Miller et al. 1998), observations or strong upper limits of non-thermal tails in atoll sources are needed to determine which, if any, of the theoretical pictures is correct. The present data are not sufficient for any strong constraints. A long integration with a sensitive hard X-ray/soft γ−ray telescope such as INTEGRAL should be able to resolve the question of the nonthermal tail.

We find results for the hard state observations that are consistent with other work (e.g. Barret et al. 1999). However, we note some systematic differences between the rising hard state and the falling hard state. Specifically, on the way into the soft state, the corona has a higher optical depth, higher compactness ratio, and a lower temperature than on the way out of the soft state. The luminosity of the source is substantially higher in rising portion of the hard state than in the falling portion of the hard state. The blackbody temperatures in the rising portion of the hard state are lower than in the falling portion. The spectral fit to a typical low/hard state observation is shown in Fig. 4.

The differences in coronal parameters of the rising and falling hard states are likely to be straightforward consequences of the luminosity difference – at higher luminosities the corona will be cooler and have a larger optical depth. Such results have been predicted theoretically (see e.g.

Esin et al. 1997). They are furthermore suggested in the black hole system XTE J 1550-564 by the hardening of the 20–100 keV spectrum as the source drops in luminosity through its low/hard state (Sobczak et al. 2000).That the luminosity is higher on the way into the soft state than on the way out indicates a hysteresis effect in the state transitions. This observation and similar observations for several black hole soft X-ray transients are discussed in another paper (Maccarone & Coppi 2003). We briefly note that this observation argues strongly against the propeller effect as the sole cause of the state transitions in Aql X-1, as propeller models predict a constant state transition luminosity, and that a single model for black hole and neutron star state transitions is instead suggested.

5. Observations of a type I burst during the hard state

We have also observed a type I X-ray burst during Observation 40047-01-01-01, shortly before the transition from the hard state to the soft state. During this burst, the PCA count rate rises by a factor of about 10, the HEXTE count rate from 15–30 keV rises by a factor of about 20% and the HEXTE count rate from 30–60 keV drops by a factor of about 2. The drop in the 30–60 keV band is significant at only the 2 σ level, but its occurrence simultaneously with the burst eliminates the possibility of "hidden trials" and allows the one-sided confidence interval of the result, i.e. 98%, to be taken literally. The light curve of this burst in the two HEXTE energy bands, binned on a 64 second timescale, is shown in Fig. 5. The burst began at $t = 169\,771\,900$ s in RXTE mission units, peaked 9 s later, and lasted about 100 s before the flux returned to the pre-burst level.

The observation of a type I X-ray burst during the hard state provides a probe for the energy content of the corona. The X-ray burst increases the soft photon luminosity by a factor of ~10, presumably without increasing the power supplied to the electrons in the corona. A uniform temperature and density spherical corona will have a total energy content of $\frac{4\pi}{3}R_{\rm cor}^3 n_e k_{\rm B}T$. Thus for a uniform temperature and density corona with $\tau > 1$, $E_{\rm cor}$, the energy content of the corona is:

$$E_{\rm cor} = 5 \times 10^{31}(y/2)(\tau/5)^{-1}\left(\frac{R_{\rm cor}}{100\,{\rm km}}\right)^2 \text{ ergs}, \tag{1}$$

where y is the Compton y parameter ($y = 4kT\max(\tau, \tau^2)/m_e c^2$), τ is the optical depth of the corona, and $R_{\rm cor}$ is the radius of the corona, and where the leading coefficient is the numerical evaluation of $\frac{2\pi}{15}\frac{(100\,{\rm km})^2}{\sigma_{\rm T}}m_e c^2$ in units of ergs. The additional seed photons in the burst should provide for additional cooling of the corona. If this additional cooling takes away an amount of energy that is comparable to the total energy content of the corona, then the temperature of the corona should drop significantly. Such a temperature drop is seen, in the form of the factor of 2 decrease in the 30–60 keV flux during the burst. Since the fluence of the burst is large (~3×10^{38} ergs), we can place only the weak limit on the corona size that it must be less than ~1 light-second in size if it has uniform temperature and density. The sensitivity of HEXTE is not sufficient to obtain strong upper limits on the corona's size from a single burst.
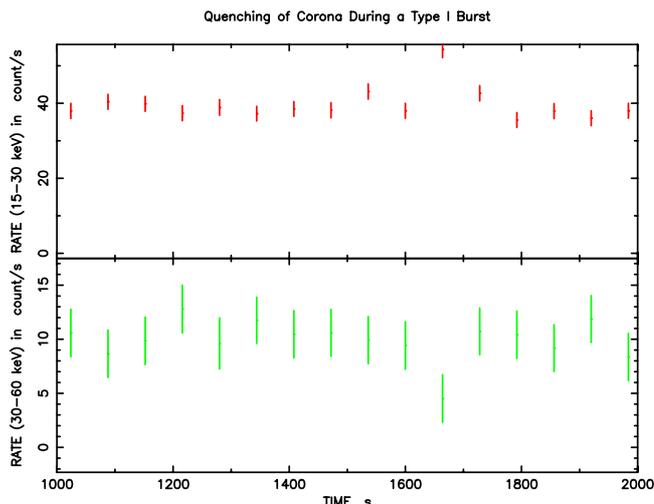
Fig. 5. The quenching of the corona during a type I X-ray burst in Observation 40047-01-01-01. The top panel shows the 15–30 keV HEXTE lightcurve, while the bottom panel shows the 30–60 keV HEXTE lightcurve. At t = 1650 s along the x-axis, the 15–30 keV band shows its flux rising due to the burst, while the 30–60 keV flux is quenched.

Stacking bursts so that a statistically significant change in the HEXTE count rate can be detected more quickly (and hence after less total soft fluence) should be a topic for future work. If future observations measure an energy content substantially lower than the current measurement, this would provide evidence for an energy reservoir in the corona other than thermal energy; a good candidate for such a reservoir would be the magnetic field (Merloni & Fabian 2001).

   The total energy emitted during the hard state observations is about 4×10^{40} ergs. The long bursts seen in the island/hard states of accreting neutron star systems are thought to be caused by the nuclear burning of hydrogen (Muno et al. 2000). Assuming an accretion efficiency of about 20%, about 2×10^{20} grams of material was accreted during that time. Assuming solar composition, about 1.5×10^{20} grams must be in the form of hydrogen, which would allow for about 10^{39} ergs to be produced by thermonuclear burning of hydrogen into helium, assuming there is no steady burning. Since the observed burst had a fluence of 3×10^{38} ergs, the expected number of bursts is about 3. If only 10% of the matter actually reaches the surface of the neutron star, as claimed in propeller model for the hard state (Zhang et al. 1998), the expected number of observed bursts would be about 0.3 (assuming bursts can occur in polar accretion models, which is uncertain); thus, the observation of a single burst does not place any tight constraints on how much matter can be propelled away from the accretion flow. Observations of bursts at lower luminosities might prove useful for constraining the luminosity at which propeller effects set in.

6. Conclusions

We have found that the spectra of Aql X-1 in all spectral states can be well fit by a pure thermal Comptonization model, but that other models, including those with substantial non-thermal electron components can also fit the data. We have find a decrease in the 30–60 keV emission coincident with a type I burst in the hard state of Aql X-1 and shown that such bursts can be used as probes of the corona's total energy content and size.

References

Arnaud, K. A. 1996, in Astronomical Data Analysis Software and Systems V, ed. G. H. Jacoby, & J. Barnes (San Francisco: ASP), ASP Conf. Ser., 101
Barret, D., & Olive, J.-F. 2002, ApJ, 576, 391
Blandford, R., & Begelman, M. C. 1999, MNRAS, 303, L1
Bradt, H. V., Rothschild, R. E., & Swank, J. H. 1993, A&AS, 97, 35
Campana, S., Stella, L., Mereghetti, S., et al. 1998, ApJ, 499, L65
Chevalier, C., Ilovaisky, S. A., Leisy, P., & Patat, F. 1999, A&A, 347, L51
Coppi, P. S. 1999, ASP Conf. Ser., 161, ed. J. Poutanen, & R. Svenson, 375
Cui, W., Barret, D., Zhang, S. N., et al. 1998, ApJ, 502, L49
D'Amico, F., Heindl, W. A., Rothschild, R. E., & Gruber, D. 2001, ApJ, 547, 147
Di Matteo, T., Celotti, A., & Fabian, A. C. 1999, MNRAS, 304, 809
di Salvo, T., Robba, R. N., Iaria, R., et al. 2001, ApJ, 554, 49
Frontera, F., Palazzi, E., Zdziarski, A. A., et al. 2001, ApJ, 546, 1027
Garcia, M. R., McClintock, J. E., Narayan, R., et al. 2001, ApJ, 553, L47
Jain, R. K. 2001, Ph.D. Thesis, Yale University
Jain, R. K., Bailyn, C. D., Garcia, M. R., & Levine, A. M., in preparation
Jain, R. K., Bailyn, C. D., Orosz, J. A., McClintock, J. E., & Remillard, R. A. 2001, ApJ, 554, L181
Lamb, F. K., Pethick, C. J., & Pines, D. 1973, ApJ, 184, 271
Maccarone, T. J., & Coppi, P. S. 2003, MNRAS, 338, 189
Merloni, A., & Fabian, A. C. 2001, MNRAS, 321, 549
Meyer, F., Liu, B. F., & Meyer-Hoffmeister, E. 2000, A&A, 354, L67
Miller, M. C., Lamb, F. K., & Psaltis, D. 1998, ApJ, 508, 791
Muno, M. P., Fox, D. W., Morgan, E. H., & Bildsten, L. 2000, ApJ, 542, 1016
Muno, M. P., Remillard, R. A., & Chakrabarty, D. 2002, ApJ, 568, L35
Nayakshin, S., & Svensson, R. 2001, ApJ, 551, L67
Narayan, R., & Yi, I. 1995, ApJ, 452, 710
Nowak, M. A. 1995, PASP, 107, 1207
Nowak, M. A., Wilms, J., & Dove, J. B. 2002, MNRAS, 332, 856
Papathanassiou, H., & Psaltis, D. 2001, to appear in MNRAS [astro-ph/0011447]
Reig, P., Mèndez, M., van der Klis, M., & Ford, E. C. 2000, ApJ, 530, 916
Rutledge, R. E., Bildsten, L., Brown, E. F., Pavlov, G. G., & Zavlin, V. E., ApJ, 559, 1054
Sobczak, G. J., McClintock, J. E., Remillard, R. A., Bailyn, C. D., & Orosz, J. A. 1999, ApJ, 520, 776
Sobczak, G. J., McClintock, J. E., Remillard, R. A., et al. 2000, ApJ, 544, 993
Titarchuk, L., & Zannias, T. 1998, ApJ, 493, 863
Yi, I., Narayan, R., Barret, D., & McClintock, J. E. 1996, A&AS, 120, 187
Zhang, S. N., Yu, W., & Zhang, W. 1998, ApJ, 494, L71